Geophysical Research Letters

RESEARCH LETTER
10.1029/2018GL080521

# Observational Constraints Reduce Likelihood of Extreme Changes in Multidecadal Land Water Availability

**Ryan S. Padrón[1], Lukas Gudmundsson[1], and Sonia I. Seneviratne[1]**

[1]Institute for Atmospheric and Climate Science, Department of Environmental Systems Science, ETH Zurich, Zurich, Switzerland

**Key Points:**
- Model differences in present-day precipitation partially explain the uncertainty of projected changes in long-term mean water availability
- A constrained ensemble reduces the likelihood of extreme changes in water availability over 73% of the global land area
- The likelihood of extreme drying is 5 times smaller in Europe, Western North America, and Southern Africa, relative to the full ensemble

**Supporting Information:**
- Supporting Information S1

**Correspondence to:**
R. S. Padrón,
ryan.padron@env.ethz.ch

**Citation:**
Padrón, R. S., Gudmundsson, L., & Seneviratne, S. I. (2019). Observational constraints reduce likelihood of extreme changes in multidecadal land water availability. *Geophysical Research Letters*, *46*, 736–744. https://doi.org/10.1029/2018GL080521

Received 17 SEP 2018
Accepted 18 DEC 2018
Accepted article online 28 DEC 2018
Published online 16 JAN 2019

**Abstract** Future changes in multidecadal mean water availability, represented as the difference between precipitation and evapotranspiration, remain highly uncertain in ensemble simulations of climate models. Here we identify a physically meaningful relationship between present-day mean precipitation and projected changes in water availability. This suggests that the uncertainty can be reduced by conditioning the ensemble on observed precipitation, which is achieved through a novel probabilistic approach that uses Approximate Bayesian Computation. Comparing the constrained with the full ensemble shows that projected extreme changes in water availability, denoted by the 5th and 95th percentile of the full ensemble, are less likely over 73% and 63% of land, respectively. There is also an overall shift toward wetter conditions over Europe, Southern Africa, and Western North America, whereas the opposite occurs over the Amazon. Finally, the constrained projections support adaptation to shifts in regional water availability as imposed by different global warming levels.

**Plain Language Summary** Human-induced emissions of greenhouse gases are warming our planet and if unabated would continue to do so. Projected climate change can affect rainfall, evapotranspiration, and streamflow and hence water availability over land. Climate model projections of future average water availability still vary substantially across different models. We find that part of this disagreement can be explained by the amount of rainfall that each model simulates for the present. In a drying region, for example, if a model has more water in the present, then the simulated loss is likely higher; whereas if it is already dry in the present, then there is only a small amount of water that can be lost. Therefore, we improve the projections by placing more confidence on the accuracy of those climate models whose average rainfall from the past decades is more similar to observed rainfall amounts. We show that previous projections of very extreme future changes in water availability are less likely to occur on 73% of the land's surface. We also provide improved projections of regional changes that are useful for the management of water resources, indicating more drying in the Amazon and less drying in Europe, Southern Africa, and Western North America.

## 1. Introduction

As our planet warms, we continue to experience changes in the global water cycle (Collins et al., 2013). Among these, changes in water availability over land are highly relevant for society and ecosystems alike. Here we focus on multidecadal averages of water availability, represented by precipitation (P) minus evapotranspiration (ET), which is equivalent to multidecadal mean runoff and often considered as a measure of renewable freshwater resources (e.g., Gudmundsson et al., 2017; Oki & Kanae, 2006). In a cautionary note, we highlight that changes in multidecadal means may not represent changes in actual water available at seasonal or shorter timescales (Kumar et al., 2013; Pendergrass & Knutti, 2018). At present, assessments of future changes in mean water availability with global climate model simulations show large uncertainties over most land regions (e.g., Greve et al., 2018; Greve & Seneviratne, 2015; Schewe et al., 2013), thus hindering efficient adaptation in water resources management.

Uncertainties of climate projections, forced by any given emission scenario of greenhouse gases, stem from both internal climate variability and structural differences between models (e.g., Deser et al., 2012). Although internal variability has been shown to influence trends in water availability for 20-year periods (Kumar et al., 2015), Greve et al. (2018) found that model uncertainty is dominating the spread of projected changes in long-term water availability. Moreover, Lorenz et al. (2018) highlight that model uncertainty is

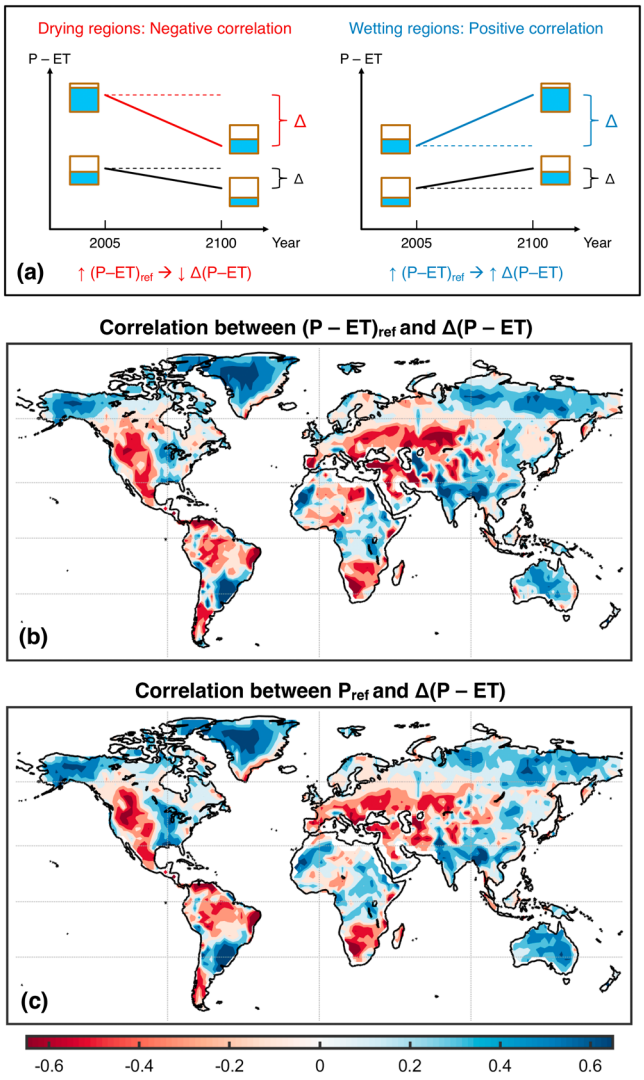


**Figure 1.** (a) Schematic representation of the hypothesized relation between present day P – ET and its future change Δ(P − ET). (b) Pearson correlation across models of $(P - ET)_{ref}$ with Δ(P − ET). (c) Pearson correlations across models of $P_{ref}$ with Δ(P − ET). Here Δ(P − ET) is the difference between the means of periods 2071–2100 and 1976–2005. P = precipitation; ET = evapotranspiration.

the best starting point to reduce the spread in climate projections. Observations are commonly used to evaluate models and constrain ensemble estimates of future hydroclimatic change, as comprehensively reviewed by Flato et al. (2013). To constrain the projections in a meaningful way, model performance needs to be evaluated against observations of a present-day quantity that can at least partially explain the differences in the model projections.

Previous research has identified relations between simulated climate characteristics and future projections of P and ET. For example, Lemordant et al. (2018) found that differences in stomatal resistance under future $CO_2$ levels can have a strong impact on the projections. However, stomatal resistance is an unsuitable variable for constraining climate models since it cannot be compared with reliable present-day observations. Li et al. (2017) identified a dependency of changes in the Indian Summer Monsoon rainfall on P in the tropical western Pacific. He and Soden (2016) found that differences between simulations in their present-day climatology of sea surface temperatures can be relevant for projected P changes, and that models with a similar P climatology tend to project similar P changes. In our study we build upon this last finding and exploit biases in present-day water availability to constrain projected changes in P – ET.

## 2. Influence of Present Conditions on Future Changes in Water Availability

We hypothesize that there are regions where present-day mean water availability, as simulated by global climate models, is among the factors influencing future changes in P – ET. To discuss reasons that support this hypothesis, let us start by considering a drying region, that is, where simulations from different models generally project a decrease in P – ET. Under this condition, our expectation is that those simulations with lower P – ET in the present period (hereafter referred to as drier reference state) are more likely to project a smaller decrease in P – ET (Figure 1a). The underlying argument is that simulations with a drier reference state have less drying potential because ET over land can normally not exceed P on multidecadal timescales (Greve et al., 2014; Kumar et al., 2015; Padrón et al., 2017), and because ET rates are reduced when soil moisture conditions are low (Koster & Suarez, 2001; Seneviratne et al., 2010). Let us now consider wetting regions, that is, where simulations project an increase in P – ET for the future. It is possible that the differences causing some simulations to have higher P – ET than others in the present will remain in the future. This can lead to a stronger increase in P – ET for simulations with a wetter reference state, for example, due to processes related to the intensification of the hydrological cycle under global warming (e.g., Held & Soden, 2006). Finally, we note that there are several examples of other bounded variables with an influence of the present-day state on future projections, such as Arctic ice extent (Liu et al., 2013; Massonnet et al., 2012), runoff (Yang et al., 2017), and carbon storage (Mystakidis et al., 2016).

To test the above-mentioned hypothesis, we consider P and ET data from climate model simulations of the fifth phase of the Coupled Model Intercomparison Project (CMIP5). For the reference period 1976–2005, we use data from historical simulations, whereas for the future period 2006–2100, we use data from simulations with the "business as usual" RCP8.5 emissions scenario (Moss et al., 2010). A total of 36 different models (or model configurations) with one initial condition simulation (i.e., the "r1i1p1" member) are considered. Data from all models are bilinearly interpolated to a common 2.5° × 2.5° grid.

Projected changes in water availability for each member *i* of the considered model ensemble are given as

$$\Delta(P-ET)_i = (P-ET)_{\mathrm{fut},i} - (P-ET)_{\mathrm{ref},i} \quad \left[\mathrm{mm\ yr^{-1}}\right], \tag{1}$$

where $(P - ET)_{ref}$ is the mean for the period 1976–2005, and $(P - ET)_{fut}$ corresponds to the mean of any 30-year period ending between 2006 and 2100. We first consider the future period 2071–2100 and compute at each grid cell the Pearson correlation coefficient between $\Delta(P - ET)$ and $(P - ET)_{ref}$ across all 36 ensemble members $i$ (Figure 1b). In many regions, the correlations support the hypothesis that projected changes in water availability depend on the present wetness state of the models. In Western North America, Europe and Southern Africa correlations are clearly negative, highlighting that simulations with higher $P - ET$ in the present generally dry more by the end of the century. Conversely, in the La Plata basin and Southern Asia, correlations are positive, suggesting that models with a wetter reference state generally have a larger increase in future water availability. These results suggest that the uncertainty in future $P - ET$ changes can be reduced by favoring models with a better historical performance for reproducing observations. Unfortunately, the observational uncertainty in present-day ET is particularly high compared to other climate variables (Mueller et al., 2013; Zeng et al., 2014). Therefore, we decide to rely solely on long-term mean P to represent the present-day wetness state. This decision is supported by the fact that the correlation across models of $\Delta(P - ET)$ with $P_{ref}$ (Figure 1c) is very similar to that with $(P - ET)_{ref}$ (Figure 1b).

## 3. Obtaining a Constrained Model Ensemble for Water Availability Projections

The uncertainty in the projections of future hydroclimatic change can be constrained by attributing more influence or a higher weight to model simulations that agree better with observed precipitation. Therefore, we require observations of present-day long-term mean P to evaluate the models. To account for some of the observational uncertainty, we consider mean P from two global gridded products: CRU TS v.4.01 (Harris et al., 2014) from the period 1976–2005 and MSWEP (Beck et al., 2017) from the period 1979–2005. These products are relatively independent; whereas CRU TS consists of interpolated gauge data, MSWEP combines gauge, satellite, and reanalysis data.

To evaluate the agreement between observations and models, we use the Continuous Ranked Probability Score (CRPS), which is designed to evaluate ensemble simulations (e.g., Jollife & Stephenson, 2012). The CRPS computes the integrated square difference between the cumulative distributions from the multimodel ensemble and the observations. Precipitation data are log-transformed when computing the CRPS to avoid excessive influence of grid cells with high P. Also, weights are assigned to each grid cell proportional to their area and the absolute magnitude of the correlation between $P_{ref}$ and $\Delta(P - ET)$. The latter ensures that the focus is on regions where the potential to constrain projected changes is the greatest. Finally, Greenland and desert regions defined by Kottek et al. (2006) are not considered when evaluating model performance, as observational P estimates are generally not reliable in these regions.

To determine the weights corresponding to each of the considered models for constraining the ensemble, we follow an approach related to Bayesian model averaging (e.g., Raftery et al., 2005; Yang et al., 2017). However, here we avoid assumptions on the distribution of model estimates and observations and instead use Markov Chain Monte Carlo (MCMC) to generate samples from a posterior distribution without knowing the likelihood function (Marjoram et al., 2003).

A general description of our methodology is presented here, whereas detailed information is provided in Supporting Information S1. In our case, the weight of each model $i$ represents the probability $\alpha_i$ of being included in the constrained ensemble. Whereas the original full ensemble corresponds to the case with $\alpha_i = 1$ for all models, our goal is to determine the values of $\alpha_i$ that minimize the CRPS (i.e., maximize the agreement between model simulations and observations). An initial set of $\alpha_i$ values is selected at random, and then the optimization of $\alpha_i$ is achieved by iterating through the following steps:

1. Propose a new set of $\alpha_i$ values as a function of their values from the previous iteration.
2. Create a model ensemble of 100 members by sampling with these probabilities $\alpha_i$.
3. Compute the agreement of the ensemble with the observations through the CRPS.
4. If the CRPS of the current iteration is smaller than the CRPS of the previous iteration, store the proposed set of $\alpha_i$; otherwise, keep the previous set and start a new iteration.

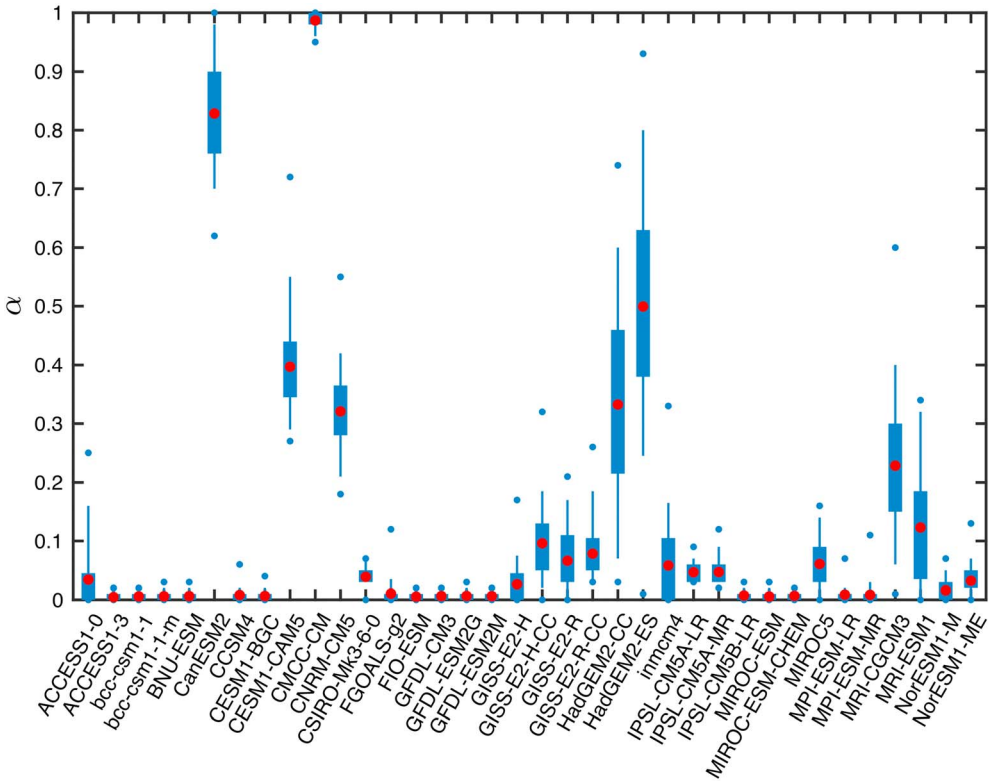


**Figure 2.** Distribution of the optimized probability ($\alpha_i$) of each model to be included in the constrained ensemble. The plotted data are obtained by optimizing $\alpha_i$ after starting from 100 different initial sets. Blue dots represent the minimum and maximum values; lines reach the 5th and 95th percentiles; and boxes cover the interquartile range. Red dots represent the mean probabilities that are used to sample the constrained ensemble.

The optimization of $\alpha_i$ is complete when it is no longer possible to reduce the resulting CRPS. In practice, we use 40,000 iterations because there is almost no improvement of the CRPS after a shorter initial phase. Additionally, to capture the possible distributions of the optimized $\alpha_i$ probabilities, we repeat the process 100 times starting from different initial sets of $\alpha_i$ chosen at random (Figure 2). The final CRPS values for all of these cases are very similar. Finally, the constrained ensemble is composed by sampling 100 times with the mean of the optimized $\alpha_i$ probabilities.

After optimizing $\alpha_i$, it becomes evident that some models are almost always included in the constrained ensemble, that is, $\alpha_i \approx 1$ (e.g., CMCC-CM and CanESM2); whereas others are instantly excluded, $\alpha_i \approx 0$ (e.g., BNU-ESM and FIO-ESM). There are also cases where the similarities and dependencies across models allow to interchange one of them for the other with minor effect on the CRPS (e.g., HadGEM2-CC with HadGEM2-ES and MRI-CGCM3 with MRI-ESM 1); this is why the variability of their optimized $\alpha_i$ is higher. For CESM1-CAM5 and CNRM-CM5, the high variability of $\alpha_i$ suggests that their inclusion in the constrained ensemble has a small effect on the agreement with observed P.

## 4. Constrained Projections of Future Changes in Water Availability

A global summary of water availability projections from the constrained ensemble for the end of the century is shown in Figure 3. Although the mean changes in P – ET are not strikingly different than what we know from the full ensemble, there are interesting differences regarding the ensemble spread. For the constrained ensemble, 44.4% of the grid cells have an absolute signal to noise ratio > 1, indicating confidence in the sign of $\Delta$(P − ET). This corresponds to an increase of 8.1% relative to the full ensemble, which is mainly attributed to a higher model agreement on a wetting of western Russia and northeast China. Furthermore, the differences in the signal-to-noise ratio indicate that the full model ensemble is overall drier than the constrained ensemble for latitudes between 30° and 60° North.

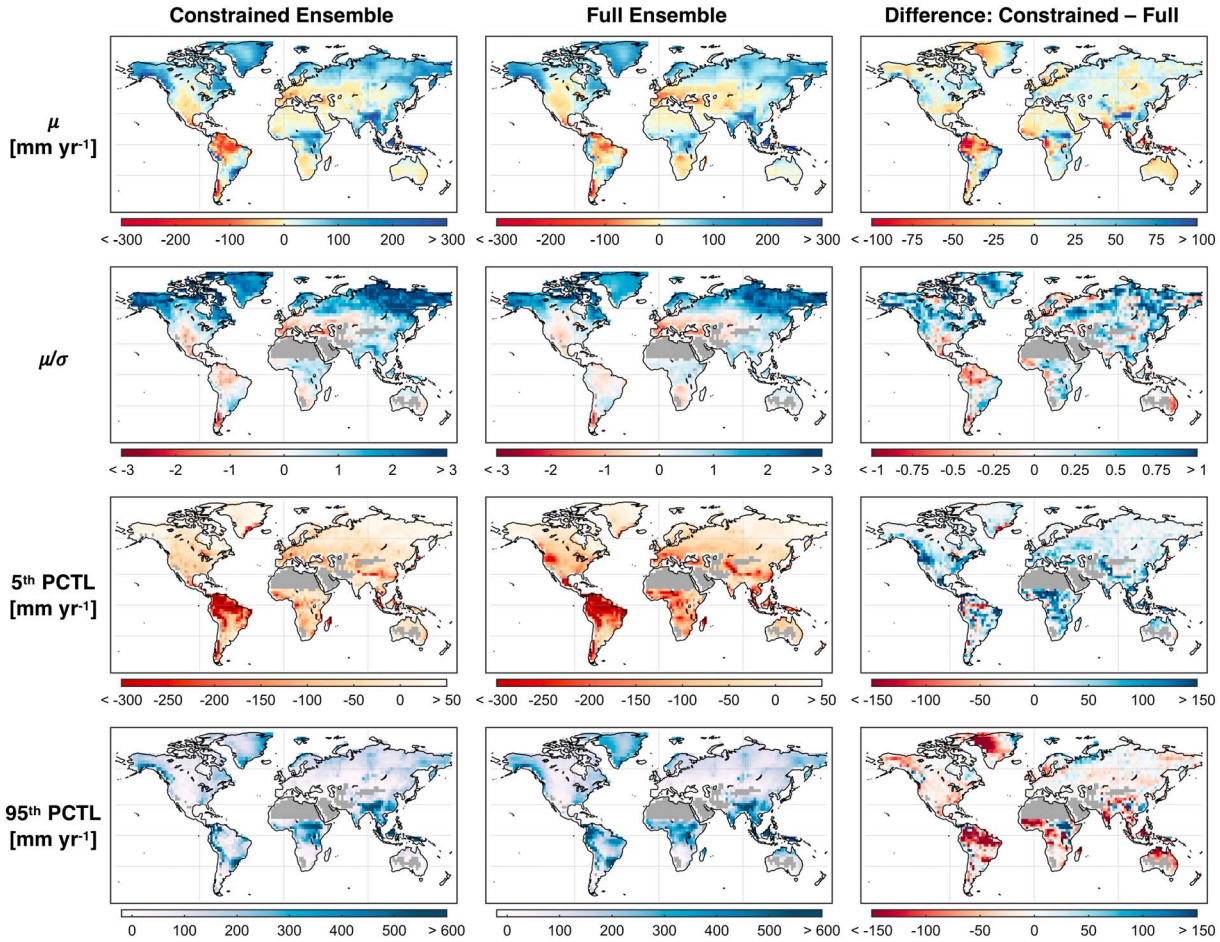


**Figure 3.** Comparison of Δ(P − ET) projections between the full and the constrained ensembles. Here Δ(P − ET) corresponds to changes between the means of periods 1976–2005 and 2071–2100 and is expressed in millimeters per year. The four rows correspond to the mean (μ), the mean-to-standard deviation ratio or signal-to-noise ratio (μ/σ), the 5th percentile (PCTL) of the ensemble, and the 95th percentile of the ensemble. P = precipitation; ET = evapotranspiration.

From a climate-impact perspective, insights on possible extreme changes are highly relevant. For this purpose, we focus on the 5th and 95th percentiles of the ensemble at each grid cell. The extreme projected drying, represented by the 5th percentile, is less intense for the constrained ensemble throughout most regions of the globe when compared to the full ensemble—this is the case in 84% of land grid cells within the latitudinal band 30–50°N. Furthermore, the reduction in the drying magnitude can be greater than 100 mm $yr^{-1}$ in hot spots like Western North America and south of the Sahara. A strong reduction in the magnitude of projected extreme wetting is also found, for example, in Western Africa, Northern South America, and Northern Australia.

Summaries of changes in regional water availability provide a more detailed view of the increased confidence obtained with the constrained ensemble. Figure 4 presents the results for selected regions from Seneviratne et al. (2012) that show a strong reduction in the ensemble spread for different global warming levels (see Figure S1 for all other regions). This analysis considers periods for which all models exhibit the same increase in global mean temperature ($\Delta Tg$) with respect to preindustrial conditions (here 1870–1899), as opposed to using fixed time windows. To put the reported values of Δ(P − ET) in each region into context, the figure also includes mean present-day water availability from the constrained ensemble. The results indicate that the constrained distributions are predominantly shifted toward wetter conditions relative to the full ensemble, although the opposite is true for the Amazon. Other relevant features of the constrained ensemble are the less severe drying for the 5th percentile in economically important regions like Western North America, Central Europe, and Southern Africa; as well as the reduced wetting for the 95th percentile in Western Africa and Southern Asia.

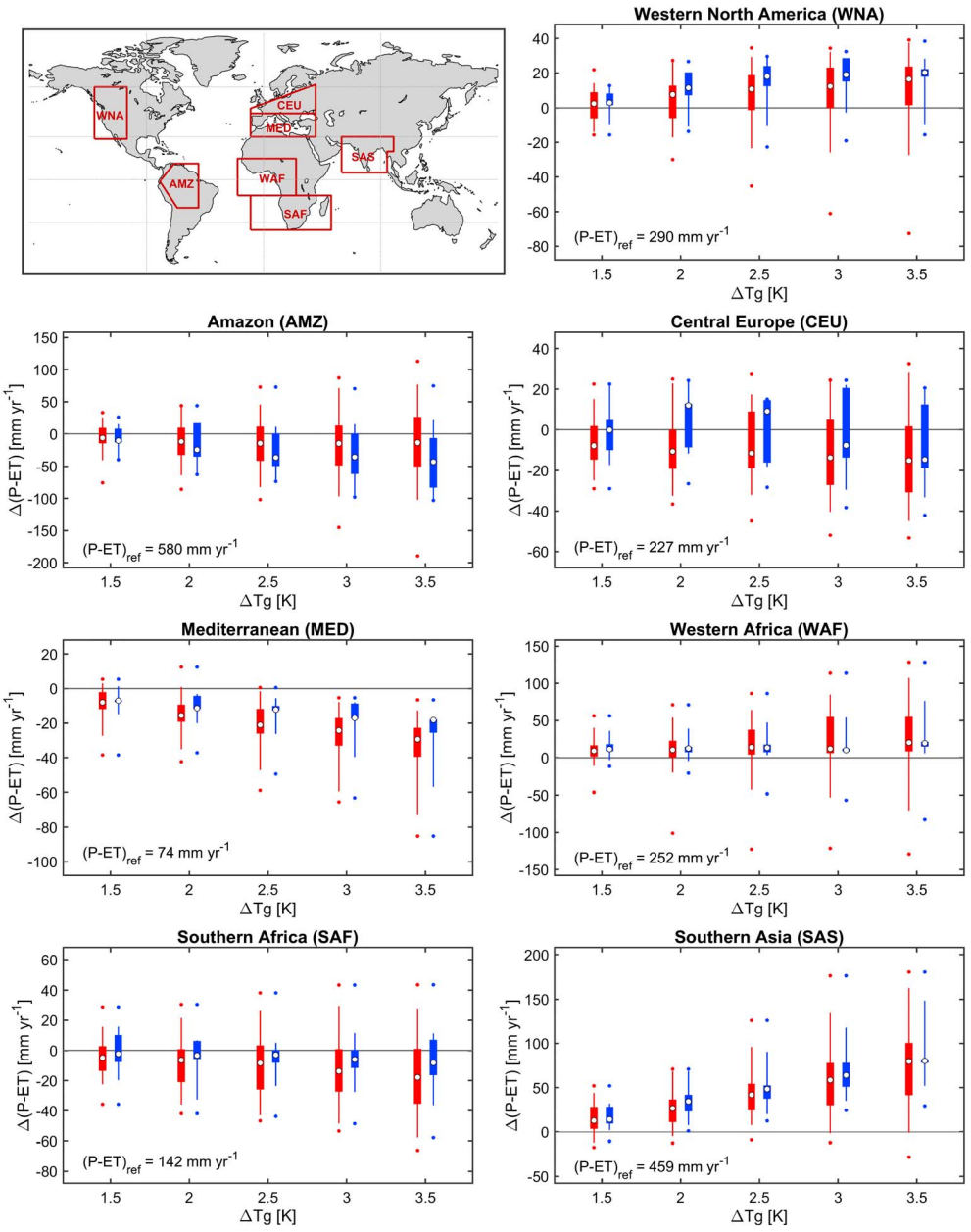


**Figure 4.** Differences between the distributions of regionally averaged Δ(P − ET) from the full model ensemble (red) and the constrained ensemble (blue) for increasing global mean temperature with respect to the preindustrial period (1870–1899). Dots represent the 1st, 50th, and 99th percentiles; lines reach the 5th and 95th percentiles; and boxes cover the interquartile range. The spatial domain of each region is shown on the top left. Regional mean present-day water availability from the constrained ensemble is indicated as $(P - ET)_{ref}$. P = precipitation; ET = evapotranspiration.

A key aspect of the constrained ensemble is the reduced likelihood of extreme changes in water availability relative to the full ensemble. To quantify this reduction, we start by defining $p_f$ as the probability of exceeding an extreme threshold in Δ(P − ET) within the full ensemble, and $p_c$ as the probability of exceeding the same threshold within the constrained ensemble. The probability ratio $PR = p_c / p_f$ can then be used to quantify the change in the likelihood of exceeding the selected threshold—for example, $PR = 1$ indicates no change, $PR = 1/2$ indicates that it is two times less likely to exceed the threshold in the constrained ensemble, and $PR = 2$ that it is two times more likely. Here we compute $PR$ by selecting the 5th and 95th percentile of Δ(P − ET) from the full ensemble as the respective thresholds to represent extreme drying

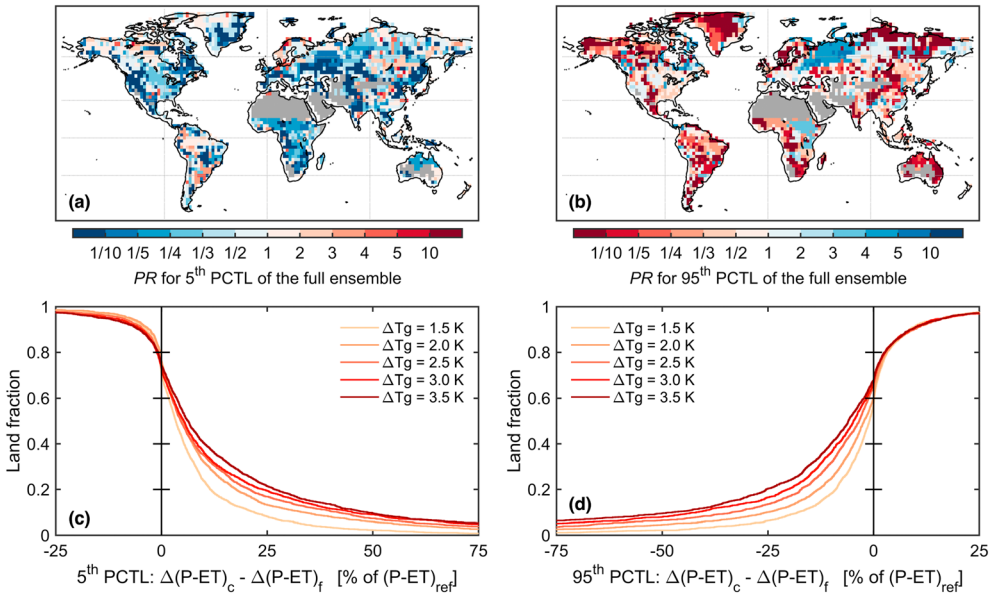


**Figure 5.** (top) Probability ratio *PR* for extreme projections of Δ(P − ET) corresponding to the 5th (a) and 95th (b) percentile (PCTL) of the full ensemble. The constrained ensemble reduces the likelihood of extreme changes when $PR < 1$. (bottom) Cumulative land fraction as function of the difference between the 5th (c) and 95th (d) percentiles of the projections from the constrained ensemble ($\Delta(P-ET)_c$) and the full ensemble ($\Delta(P-ET)_f$). Differences are shown relative to mean present-day P – ET from the constrained ensemble. Positive values in the *X* axis of (c) indicate less extreme drying in the constrained ensemble. Negative values in the *X* axis of (d) indicate less extreme wetting in the constrained ensemble. Each line in the plots corresponds to a different mean global warming level with respect to the preindustrial period (1870–1899). Greenland and desert regions are excluded from this analysis. P = precipitation; ET = evapotranspiration.

and wetting. For both cases, $p_f = 0.05$, while $p_c$ is obtained at each grid cell from the magnitude of the corresponding thresholds.

Global maps of *PR* highlight the strong reduction of the likelihood of extreme Δ(P − ET) for the constrained ensemble, with values below 1/5 in several regions (Figure 5). Note, however, that there is an increased likelihood of extreme drying in parts of the Amazon, as well as of extreme wetting in Eastern Africa and Western Russia. To complement these results, we compute the global cumulative distribution of the differences between the 5th percentiles of the constrained and full ensemble and also between the 95th percentiles. Results for the 5th percentile indicate that extreme drying is reduced in approximately 73% of land grid cells, with low dependence on global warming levels. Furthermore, in 25% of all land grid cells, the reduction for a 3 K global warming is greater than 18% of mean present-day P – ET. Finally, extreme wetting is also substantially reduced in the constrained ensemble, although to a slightly smaller degree than extreme drying.

## 5. Conclusions

This study describes how present-day mean precipitation in climate models influences projections of future changes in multidecadal mean P minus ET. We identify regions such as Western North America, Central Europe, the Mediterranean, and Southern Africa, where a wetter reference state in the models is negatively correlated to the projected change in P – ET. This suggests that model simulations with high present-day water availability often dry more under global warming in these regions; whereas if water availability is already low, it is less likely to decrease and might even increase. On the other hand, the intensification of the hydrologic cycle with global warming may explain why simulations with wetter conditions in the present tend to project a larger increase in P – ET in regions with high P, such as Southern Asia and La Plata basin in South America. Based on the relevance of the reference state, we argue that simulations that agree better with observations are likely more reliable for future projections.

To evaluate and to constrain the considered model ensemble, a novel approach that is based on quantifying the probability of each model to be included in a constrained ensemble is introduced. The distributions of these probabilities help to identify models with evident agreement with observations and models with evident disagreement, as well as the ability of the method to account for very similar models. Furthermore, the presented algorithm is applicable to cases involving different constraining metrics, and it can incorporate both multiple ensemble simulations per model and multiple observational products. Finally, it is important to recall that while our study focuses on reducing uncertainty stemming from differences between climate models, emission scenarios and internal variability might also influence the spread of the projections.

The resulting constrained estimates of projected changes in long-term mean P – ET generally show a narrower distribution compared to the full model ensemble, together with a shift in the distribution toward wetter conditions in several regions around the world. However, there is an increased likelihood for drying in the Amazon. We highlight that the constrained ensemble suggests a reduced likelihood of extreme drying over most of the land surface. This is especially noteworthy and relevant for Europe, Southern Africa, and Western North America. Nonetheless, this reduction in drying does not necessarily imply that strong drying is not possible; for example, 5% (25%) of the constrained ensemble members still project a decrease in water availability relative to the present-day ensemble mean of up to 53.3% (23.6%) in the Mediterranean and 19.4% (8.2%) in Southern Africa, under a 3 K global warming. The reduced uncertainty in multidecadal mean water availability projections obtained in this study is highly relevant for climate adaptation and decision making.

**Acknowledgments**
We acknowledge partial support from the H2020 CRESCENDO project (grant agreement 641816) and from the European Research Council (ERC) DROUGHT-HEAT project funded by the European Community's Seventh Framework Programme (grant agreement FP7-IDEAS-ERC-617518). We acknowledge the World Climate Research Program's Working Group on Coupled Modeling, which is responsible for the Coupled Model Intercomparison Project (CMIP), and we thank the climate modeling groups for producing and making available their model output. For CMIP, the U.S. Department of Energy's Program for Climate Model Diagnosis and Intercomparison provides coordinating support and led development of software infrastructure in partnership with the Global Organization for Earth System Science Portals. The CMIP5 data used in this study are available at https://esgf-node.llnl.gov/projects/esgf-llnl/. Precipitation data from CRU TS are available at https://crudata.uea.ac.uk/cru/data/hrg/cru_ts_4.01/ and from MSWEP at http://www.gloh2o.org. We thank Urs Beyerle and Jan Sedlacek for processing the CMIP5 data.

## References

Beck, H. E., van Dijk, A. I. J. M., Levizzani, V., Schellekens, J., Miralles, D. G., Martens, B., & de Roo, A. (2017). MSWEP: 3-hourly 0.25° global gridded precipitation (1979–2015) by merging gauge, satellite, and reanalysis data. *Hydrology and Earth System Sciences*, *21*(1), 589–615. https://doi.org/10.5194/hess-21-589-2017

Collins, M., Knutti, R., Arblaster, J., Dufresne, J.-L., Fichefet, T., Friedlingstein, P., et al. (2013). Long-term climate change: Projections, commitments and irreversibility. In T. F. Stocker, D. Qin, G.-K. Plattner, M. Tignor, S. K. Allen, J. Boschung, et al. (Eds.), *Climate change 2013: The physical science basis. Contribution of Working Group I to the Fifth Assessment Report of the Intergovernmental Panel on Climate Change* (Chapter 12, pp. 1029–1136). Cambridge, United Kingdom and New York, NY: Cambridge University Press.

Deser, C., Phillips, A., Bourdette, V., & Teng, H. (2012). Uncertainty in climate change projections: The role of internal variability. *Climate Dynamics*, *38*(3–4), 527–546. https://doi.org/10.1007/s00382-010-0977-x

Flato, G., Marotzke, J., Abiodun, B., Braconnot, P., Chou, S. C., Collins, W., et al. (2013). Evaluation of climate models. In T. F. Stocker et al. (Eds.), *Climate change 2013: The physical science basis. Contribution of Working Group I to the Fifth Assessment Report of the Intergovernmental Panel on Climate Change* (Chapter 9, pp. 741–866). Cambridge, United Kingdom and New York, NY: Cambridge University Press.

Greve, P., Gudmundsson, L., & Seneviratne, S. I. (2018). Regional scaling of annual mean precipitation and water availability with global temperature change. *Earth System Dynamics*, *9*(1), 227–240. https://doi.org/10.5194/esd-9-227-2018

Greve, P., Orlowsky, B., Mueller, B., Sheffield, J., Reichstein, M., & Seneviratne, S. I. (2014). Global assessment of trends in wetting and drying over land. *Nature Geoscience*, *7*(10), 716–721. https://doi.org/10.1038/ngeo2247

Greve, P., & Seneviratne, S. I. (2015). Assessment of future changes in water availability and aridity. *Geophysical Research Letters*, *42*, 5493–5499. https://doi.org/10.1002/2015GL064127

Gudmundsson, L., Seneviratne, S. I., & Zhang, X. (2017). Anthropogenic climate change detected in European renewable freshwater resources. *Nature Climate Change*, *7*(11), 813–816. https://doi.org/10.1038/nclimate3416

Harris, I., Jones, P. D., Osborn, T. J., & Lister, D. H. (2014). Updated high-resolution grids of monthly climatic observations—The CRU TS3.10 dataset. *International Journal of Climatology*, *34*(3), 623–642. https://doi.org/10.1002/joc.3711

He, J., & Soden, B. J. (2016). The impact of SST biases on projections of anthropogenic climate change: A greater role for atmosphere-only models? *Geophysical Research Letters*, *43*, 7745–7750. https://doi.org/10.1002/2016GL069803

Held, I., & Soden, B. (2006). Robust responses of the hydrological cycle to global warming. *Journal of Climate*, *19*(21), 5686–5699. http://journals.ametsoc.org/doi/abs/10.1175/JCLI3990.1

Jollife, I. T., & Stephenson, D. B. (2012). *Forecast verification. A practitioner's guide in atmospheric science* (2nd ed., University of Exeter). UK: Wiley-Blackwell.

Koster, R. D., & Suarez, M. J. (2001). Soil moisture memory in climate models. *Journal of Hydrometeorology*, *2*(6), 558–570. https://journals.ametsoc.org/doi/pdf/10.1175/1525-7541%282001%29002%3C0558%3ASMMICM%3E2.0.CO%3B2

Kottek, M., Grieser, J., Beck, C., Rudolf, B., & Rubel, F. (2006). World map of the Köppen-Geiger climate classification updated. *Meteorologische Zeitschrift*, *15*(3), 259–263. https://doi.org/10.1127/0941-2948/2006/0130

Kumar, S., Allan, R. P., Zwiers, F., Lawrence, D. M., & Dirmeyer, P. A. (2015). Revisiting trends in wetness and dryness in the presence of internal climate variability and water limitations over land. *Geophysical Research Letters*, *42*, 10,867–10,875. https://doi.org/10.1002/2015GL066858

Kumar, S., Lawrence, D. M., Dirmeyer, P. A., & Sheffield, J. (2013). Less reliable water availability in the 21st century climate projections. *Earth's Future*, *2*, 152–160. https://doi.org/10.1002/2013EF000159

Lemordant, L., Gentine, P., Swann, A. S., Cook, B. I., & Scheff, J. (2018). Critical impact of vegetation physiology on the continental hydrologic cycle in response to increasing $CO_2$. *Proceedings of the National Academy of Sciences of the United States of America*, *115*(16), 4093–4098. https://doi.org/10.1073/pnas.1720712115

Li, G., Xie, S.-P., He, C., & Chen, Z. (2017). Western Pacific emergent constraint lowers projected increase in Indian summer monsoon rainfall. *Nature Climate Change*, *7*(10), 708–712. https://doi.org/10.1038/nclimate3387

Liu, J., Song, M., Horton, R. M., & Hu, Y. (2013). Reducing spread in climate model projections of a September ice-free Arctic. *Proceedings of the National Academy of Sciences of the United States of America*, *110*(31), 12,571–12,576. https://doi.org/10.1073/pnas.1219716110

Lorenz, R., Herger, N., Sedláček, J., Eyring, V., Fischer, E. M., & Knutti, R. (2018). Prospects and caveats of weighting climate models for summer maximum temperature projections over North America. *Journal of Geophysical Research: Atmospheres.*, *123*, 4509–4526. https://doi.org/10.1029/2017JD027992

Marjoram, P., Molitor, J., Plagnol, V., & Tavare, S. (2003). Markov chain Monte Carlo without likelihoods. *Proceedings of the National Academy of Sciences of the United States of America*, *100*(26), 15,324–15,328. https://doi.org/10.1073/pnas.0306899100

Massonnet, F., Fichefet, T., Goosse, H., Bitz, C. M., Philippon-Berthier, G., Holland, M. M., & Barriat, P.-Y. (2012). Constraining projections of summer Arctic sea ice. *The Cryosphere*, *6*(6), 1383–1394. https://doi.org/10.5194/tc-6-1383-2012

Moss, R. H., Edmonds, J. A., Hibbard, K. A., Manning, M. R., Rose, S. K., van Vuuren, D. P., et al. (2010). The next generation of scenarios for climate change research and assessment. *Nature*, *463*(7282), 747–756. https://doi.org/10.1038/nature08823

Mueller, B., Hirschi, M., Jimenez, C., Ciais, P., Dirmeyer, P. A., Dolman, A. J., Fisher, J. B., et al. (2013). Benchmark products for land evapotranspiration: LandFlux-EVAL multi-data set synthesis. *Hydrology and Earth System Sciences*, *17*(10), 3707–3720. https://doi.org/10.5194/hess-17-3707-2013

Mystakidis, S., Davin, E. L., Gruber, N., & Seneviratne, S. I. (2016). Constraining future terrestrial carbon cycle projections using observation-based water and carbon flux estimates. *Global Change Biology*, *22*(6), 2198–2215. https://doi.org/10.1111/gcb.13217

Oki, T., & Kanae, S. (2006). Global hydrological cycles and world water resources. *Science (New York, N.Y.)*, *313*(5790), 1068–1072. https://doi.org/10.1126/science.1128845

Padrón, R. S., Gudmundsson, L., Greve, P., & Seneviratne, S. I. (2017). Large-scale controls of the surface water balance over land: Insights from a systematic review and meta-analysis. *Water Resources Research*, *53*, 9659–9678. https://doi.org/10.1002/2017WR021215

Pendergrass, A. G., & Knutti, R. (2018). The uneven nature of daily precipitation and its change. *Geophysical Research Letters*, *45*, 11,980–11,988. https://doi.org/10.1029/2018GL080298

Raftery, A. E., Gneiting, T., Balabdaoui, F., & Polakowski, M. (2005). Using Bayesian model averaging to calibrate forecast ensembles. *Monthly Weather Review*, *133*(5), 1155–1174. https://doi.org/10.1175/MWR2906.1

Schewe, J., Heinke, J., Gerten, D., Haddeland, I., Arnell, N. W., Clark, D. B., et al. (2013). Multimodel assessment of water scarcity under climate change. *Proceedings of the National Academy of Sciences of the United States of America*, *111*(9), 3245–3250. https://doi.org/10.1073/pnas.1222460110

Seneviratne, S. I., Corti, T., Davin, E. L., Hirschi, M., Jaeger, E. B., Lehner, I., et al. (2010). Investigating soil moisture-climate interactions in a changing climate: A review. *Earth-Science Reviews*, *99*(3–4), 125–161. https://doi.org/10.1016/j.earscirev.2010.02.004

Seneviratne, S. I., Nicholls, N., Easterling, D., Goodess, C. M., Kanae, S., Kossin, J., et al. (2012). Changes in climate extremes and their impacts on the natural physical environment. In C. B. Field, V. Barros, T. F. Stocker, D. Qin, D. J. Dokken, K. L. Ebi, et al. (Eds.), *Managing the risks of extreme events and disasters to advance climate change adaptation A Special Report of Working Groups I and II of the Intergovernmental Panel on Climate Change (IPCC)* (pp. 109–230). Cambridge, UK, and New York, NY: Cambridge University Press. https://doi.org/10.1017/CBO9781139177245.006

Yang, H., Zhou, F., Piao, S., Huang, M., Chen, A., Ciais, P., Li, Y., et al. (2017). Regional patterns of future runoff changes from Earth system models constrained by observation. *Geophysical Research Letters*, *44*, 5540–5549. https://doi.org/10.1002/2017GL073454

Zeng, Z., Wang, T., Zhou, F., Ciais, P., Mao, J., Shi, X., & Piao, S. (2014). A worldwide analysis of spatiotemporal changes in water balance-based evapotranspiration from 1982 to 2009. *Journal of Geophysical Research: Atmospheres*, *119*, 1186–1202. https://doi.org/10.1002/2013JD020941